buildings

MDPI

Article

Post-Fire Seismic Performance of Concrete-Filled Steel Tube Frame Structures Considering Soil-Structure Interaction (SSI)

Weiwei Wang [1], Xuetao Lyu [2,*], Jun Zheng [1], Shanchang Yi [3], Jiehong Li [4] and Yang Yu [4,*]

[1] School of Architectural Engineering, Guangzhou Vocational and Technical University of Science and Technology, Guangzhou 510000, China; wangweiwei@gkd.edu.cn (W.W.); zhengjun@gkd.edu.cn (J.Z.)
[2] School of Transportation and Civil Engineering, Foshan University of Science and Technology, Foshan 528231, China
[3] School of Civil Engineering, Changsha University of Science & Technology, Changsha 410114, China; shanchang.yi@stu.csust.edu.cn
[4] Centre for Infrastructure Engineering and Safety, School of Civil and Environmental Engineering, The University of New South Wales, Kensington, NSW 2052, Australia; jiehong.li@unsw.edu.au
* Correspondence: lxtwww30@fosu.edu.cn (X.L.); yang.yu12@unsw.edu.au (Y.Y.)

Abstract: Currently, reinforced thin-walled irregular steel tube concrete frame structures have been applied in engineering, but there are few researches on the seismic performance of this type of structures after fire. The seismic performance of structures after fire is generally carried out based on rigid foundation conditions. Therefore, it is of certain engineering and theoretical value to study the seismic performance considering the SSI (soil–structure interaction) in this paper. ABAQUS is employed to establish the finite element models of the reinforced thin-walled irregular steel tube concrete frame structure considering the SSI after a fire. The paper analyzes the impact of different site conditions and fire durations on the structural natural vibration period, maximum acceleration, inter-story shear force, and maximum inter-story displacement angle. The results show that the consideration of the SSI increases the basic natural vibration period of the structure by 10–30%. The softer the soil and the longer the fire duration, the more significant the increase. For harder soil, lower seismic intensity, and shorter fire duration, the acceleration assigned to the structure and foundation after considering the SSI is smaller than the results assuming a rigid foundation. The change in inter-story shear force is mainly determined by the acceleration of the structure and foundation. The inter-story displacement angle increases when considering the SSI, and the increase is more significant with softer soil, larger seismic wave acceleration amplitude, and longer fire duration.

Keywords: post fire; SSI effect; thin-walled special-shaped steel tube concrete; framework; seismic performance

Citation: Wang, W.; Lyu, X.; Zheng, J.; Yi, S.; Li, J.; Yu, Y. Post-Fire Seismic Performance of Concrete-Filled Steel Tube Frame Structures Considering Soil-Structure Interaction (SSI). *Buildings* **2024**, *14*, 555. https://doi.org/10.3390/buildings14020555

Academic Editor: Francesco Ascione

Received: 16 January 2024
Revised: 5 February 2024
Accepted: 9 February 2024
Published: 19 February 2024

1. Introduction

Cold-formed thin-walled steel is used as the external tube for thin-walled steel tube concrete, with a diameter-to-thickness ratio or width-to-thickness ratio greater than 1.5 times the local stability limit of the hollow steel tube in compressed members [1,2]. To enhance the lateral restraint of the steel tube on the core concrete, internal stiffening steel bars are added to form a stiffened thin-walled steel tube concrete. This structure has high load-carrying capacity, stiffness, and seismic performance while saving about 35% of steel [3–5]. Common cross-sectional shapes include circular, rectangular, L-shaped, T-shaped, cross-shaped, etc. Compared to traditional sections, L-shaped, T-shaped, and cross-shaped profiles can integrate with walls, not only increasing the usable area of rooms but also facilitating furniture layout. At present, this type of structure has been used in engineering.

Fire and earthquake are two kinds of disasters with high frequency. After fire, the performance of building materials will deteriorate to different degrees, which will reduce the bearing capacity and stiffness of structures and components. In additional, rigid

foundation is generally assumed as the basic assumption for seismic analysis of structures. But the SSI exists objectively, and dynamic response of structures considering the SSI is different from rigid foundation. Therefore, it is of engineering application value to conduct research on the reinforced thin-walled irregular steel tube concrete frame structures after fire considering the SSI.

Some scholars have studied the seismic performance of special-shaped concrete-filled steel tube structures at normal temperature. Xu et al. [6] conducted quasi-static experimental research on a plane frame with four types of steel beam-concrete-filled steel tube irregular columns. Zhang et al. [7] investigated the quasi-static behavior of a frame with four two-story single-span steel beams and L-shaped steel tube concrete columns. The seismic performance of a structure with concrete-filled steel tube irregular columns was analyzed [8]. Jiang [9] studied the seismic performance of assembled steel tube concrete irregular columns in frame structures.

The seismic performance of structures after fire has been studied by some scholars. Research was conducted on post-fire seismic behavior of two-bay two-story frames with high-performance fiber-reinforced cementitious composite joints [10]. Xiong et al. [11] studied the post-fire seismic performance of composite shear walls filled with demolished concrete lumps and self-compacting concrete. Ni et al. [12] investigated the post-fire seismic performance of reinforced concrete shear wall structures. Demir et al. [13] examined the influence of post-fire time on the seismic performance of reinforced concrete structures. Post-fire seismic performance analysis was performed on multi-story reinforced concrete frames under near-fault earthquakes [14]. The seismic performance of concrete frames after local fires was studied [15].

Scholars generally use shaking table test and numerical simulation to carry out the effect of SSI on structures [16–21]. Yang et al. [22] explored the seismic performance of a 10-story concrete frame structure with sticky dampers considering the site–structure interaction (SSI). Through a six-story frame structure shake table model test considering the SSI, Liu et al. [23] studied the vibration control capability of eddy current-tuned mass dampers. Deb et al. [24] conducted shake table tests on the interaction between soil, pile foundations, and structures under soft clay field conditions. The shake table tests were conducted on the dynamic interaction between structures, piles, and soil, as well as on the mechanism of the SSI on the dynamic response of high-rise structures on rigid foundations. [25,26] conducted overall shake table tests on a scaled "wind turbine tower-foundation-soil" system considering the SSI, analyzing the impact of the SSI on the dynamic characteristics, acceleration response, and displacement response of the wind turbine tower model structure. A simplified model of large pile groups and super-tall buildings considering the SSI was established, and the dynamic response of super-tall buildings to wind loads considering the SSI was investigated [27]. Sadek et al. [28] analyzed the influence of soil–structure interaction on the natural frequency of shear wall structures. The seismic collapse capacity of steel frame structures considering the SSI was studied [29]. Using typical soft rock foundations, Zhao et al. [30] performed seismic vulnerability analysis through Incremental Dynamic Analysis (IDA). Ding et al. [29] conducted overall shake table tests on a scaled "wind turbine tower-foundation-soil" system considering the SSI, analyzing the impact of the SSI effects on the dynamic characteristics, acceleration response, and displacement response of the wind turbine tower model structure.

In summary, the study of seismic performance of composite structures is based on rigid foundation condition, and the study of thin-walled concrete-filled steel tube structures is rare; the study of structural seismic performance after fire is also mainly based on rigid foundation condition; the research on SSI mainly focuses on steel structures and concrete structures. Therefore, the seismic performance of the reinforced thin-walled irregular steel tube concrete frame structures after fire is studied in order to enrich the relevant theories of post-fire repair.

In order to study post-fire seismic performance of the reinforced thin-walled irregular steel tube concrete frame structures, this paper initially validated a mechanical finite element

models of a six-story steel frame structure considering SSI and a temperature field finite element models of post-fire reinforced thin-walled T-shaped steel tube concrete. Then, a finite element model was established for a post-fire reinforced thin-walled irregular steel tube concrete frame structure considering the SSI. The study illustrated the influence patterns of site conditions and fire exposure time on the structural natural vibration period, maximum acceleration, inter-story shear force, and maximum inter-story displacement angle.

2. Finite Element Model Validation

In view of the lack of post-fire seismic performance tests related to the SSI for composite structures, we first conducted model validation for steel frames considering the SSI at normal temperature. Subsequently, temperature field model validation for T-shaped stiffened thin-walled steel-concrete tubes was performed to ensure the effectiveness of the finite element model.

2.1. Validation of Frame Models Considering the SSI

ABAQUS simulation verification was conducted for a six-story steel frame structure as described in [31]. The steel frame beams and columns, floor slabs, independent foundations, and soil were modeled using B32, S4R, and C3D8R elements, respectively. The steel material was represented using a bilinear elastic-plastic model with a strength grade of Q235. The stress-increment-to-strain-increment ratio in the strengthening segment was 1/100. The material properties included a density of 7850 kg/m^3, an elastic modulus of 210 GPa, a Poisson's ratio of 0.3, and a yield strength of 235 MPa. The concrete was modeled using the CDP model with a strength grade of C30, a density of 2500 kg/m^3, a shear dilation angle of 15°, an eccentricity of 0.1, a Poisson's ratio of 0.167, a biaxial-to-uniaxial compressive strength ratio of 1.16, a cohesion coefficient of 0.005, and a ratio of the second stress invariant to the second invariant of stress applied in the meridian plane of 0.667. The soil was modeled using the M-C constitutive model with parameter values consistent with [31]. The reinforcement ratio for the floor slabs and foundations was set to 2%. Rayleigh damping was applied to the soil with a damping ratio of 0.08, and direct modal damping with a damping ratio of 0.05 was applied to the structure. The calculation domain for the foundation extended to 240 m × 240 m × 50 m, with isotropic three-dimensional consistent viscoelastic artificial boundaries applied at the bottom and side boundaries [32], and a free boundary at the top. Solid elements C3D8R were used for boundary elements with a thickness of 5 m, and boundary parameters α_T = 0.667, α_N = 1.333 were applied [32]. The seismic input matched that of [31]. A face-to-face contact approach was employed for modeling the contact surfaces between the foundation and the soil, with a hard contact in the normal direction and a Coulomb friction model in the tangential direction with a friction coefficient of 0.3 [31]. The foundation was modeled as 3 m × 3 m. The mesh size for the upper structure was set to 0.03 m. The verification results for the fundamental period of vibration and maximum base shear under different site conditions are presented in Table 1. The maximum inter-story displacement angles calculated along the X and Y directions of the seismic wave [31] are shown in Table 2. As can be seen from Tables 1 and 2, the calculation error of the basic natural vibration period is 2–12%, and the error of the displacement angle between each layer is about 10%, which is in good agreement. However, the simulation error of the maximum shear force of the base considering is about 20%. This may be due to the relative complexity of the contact surface between the base.

Table 1. Verification of natural vibration period and the maximum shear force of the base.

Venue Type	Basic Natural Period/s			Base Shear/kN		
	Documentation Value [31]	Simulation Value	Documentation Value/Simulation Value	Documentation Value [31]	Simulation Value	Documentation Value/Simulation Value
Rigid foundation	0.61	0.62	1.021	2274.33	2385.46	1.049
Medium hard soil	1.08	1.14	1.057	1256.28	1550.55	1.234
Medium soft soil	1.11	0.97	0.876	1168.01	1455.14	1.246
Weak soil	1.21	1.15	0.953	928.88	1192.73	1.284

Table 2. Verification results of the maximum inter-story displacement angle of each layer.

Direction	Layers	Rigid Foundation Documentation Value [31]	Calculated Value	Medium Hard Soil Documentation Value [31]	Calculated Value	Medium Soft Soil Documentation Value [31]	Calculated Value	Weak Soil Documentation Value [31]	Calculated Value
X	6	0.71%	0.86%	1.02%	1.08%	1.34%	1.36%	2.25%	2.09%
	5	0.87%	0.95%	1.09%	1.11%	1.43%	1.45%	2.28%	2.10%
	4	1.07%	1.18%	1.19%	1.24%	1.56%	1.55%	2.29%	2.19%
	3	1.43%	1.30%	1.30%	1.35%	1.69%	1.65%	2.39%	2.36%
	2	1.38%	1.40%	1.36%	1.40%	1.76%	1.68%	2.49%	2.40%
	1	1.27%	1.42%	1.40%	1.46%	1.80%	1.78%	2.57%	2.47%
Y	6	0.15%	0.15%	0.27%	0.28%	0.56%	0.62%	1.61%	1.50%
	5	0.25%	0.30%	0.36%	0.40%	0.66%	0.70%	1.61%	1.54%
	4	0.41%	0.52%	0.52%	0.58%	0.82%	0.90%	1.62%	1.57%
	3	0.73%	0.65%	0.71%	0.71%	1.00%	1.07%	1.63%	1.58%
	2	0.69%	0.65%	0.81%	0.80%	1.10%	1.18%	1.65%	1.60%
	1	0.59%	0.70%	0.84%	0.88%	1.14%	1.25%	1.66%	1.67%

2.2. Verification of the Temperature Field Model for T-Shaped Thin-Walled Steel Tube Reinforced Concrete after a Fire

A simulation validation of the post-fire heating and cooling test for T-shaped thin-walled steel tube reinforced concrete as described in [33] using ABAQUS was conducted. The thermal parameters for steel and concrete were based on the recommendations of EC4 [34]. The initial temperature for the temperature field model was set at 20 °C, with a thermal radiation coefficient of 0.7 and a thermal convective coefficient of 25 W/(m^2·°C). Thermal convection and radiation were neglected, and adiabatic conditions were applied at the column ends. Face-to-face contact was employed to simulate the contact thermal resistance between the steel tube and concrete, with concrete as the active surface and a contact thermal resistance of 0.01 (m^2·°C)/W. A tied constraint connection was used between the steel bars and concrete, and the effect of shrinkage thermal resistance was ignored. DC3D8, DS4, and DC1D2 were used for modeling the concrete, steel tube, and steel bars, respectively. The structured mesh size was set to 30 mm, as shown in Figure 1. The temperature curves for the validation points are depicted in Figure 2. As can be seen from the figure, part of the data of measuring points (d) 6 and (e) 5 were missing due to thermocouple failure during test. In general, the finite element results agreed well with the experimental results. Individual results had slightly larger errors due to: simulations were based on ideal conditions; However, in fact, there may be some problems such as local concrete placement, vent holes or steel welding in the specimen.

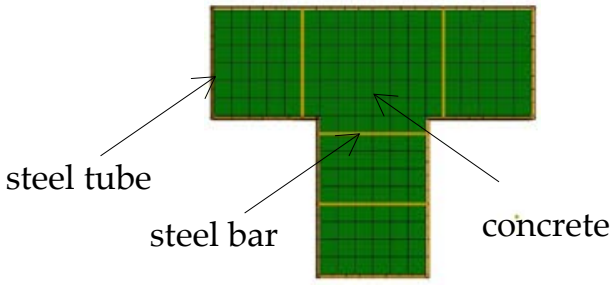

Figure 1. Grid division.

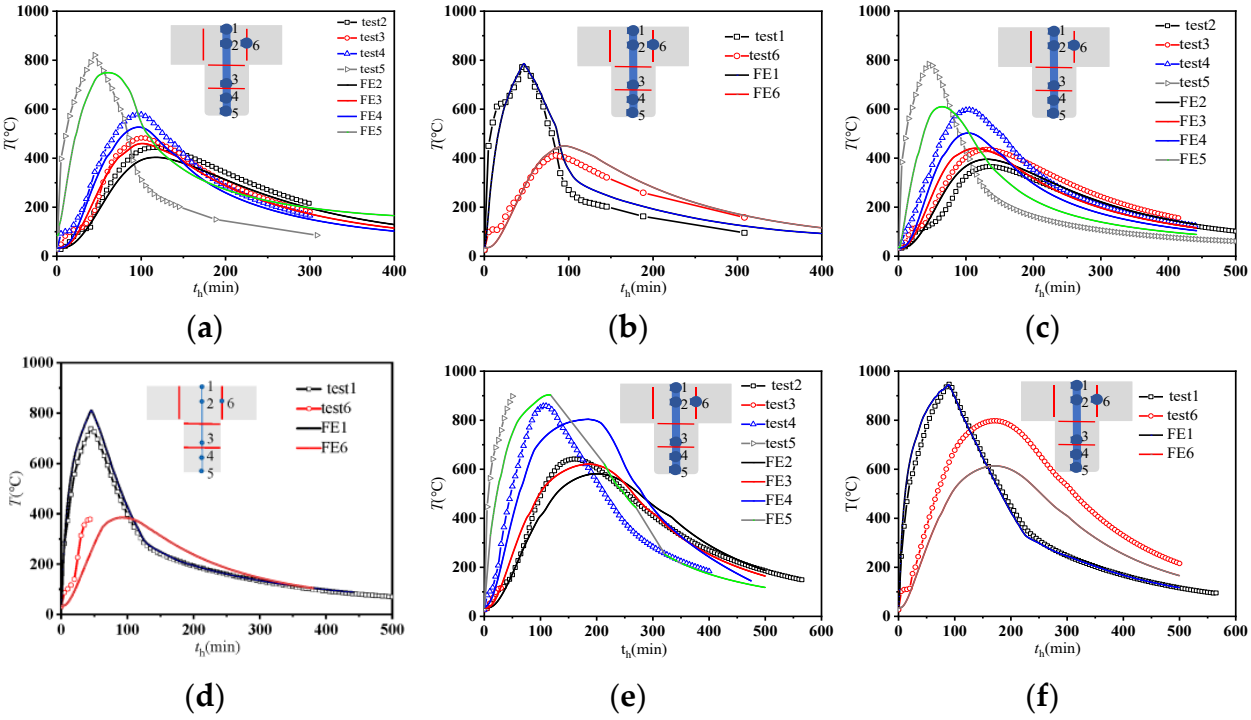

Figure 2. Verification of the temperature curve: (**a**) The first group of concrete measuring points; (**b**) The first group of steel bar measuring points; (**c**) The second group of concrete measuring points; (**d**) The second group of steel bar measuring points; (**e**) The third group of concrete measuring points; (**f**) The third group of steel bar measuring points.

3. Finite Element Model of Post-Fire Reinforced Thin-Walled Irregular Steel Tube Concrete Frame Structure Considering the SSI

As shown in Figure 3, a five-story frame structure with a height of 4.0 m for the ground floor and a standard floor height of 3.0 m. The basic information for the components is provided in Table 3.

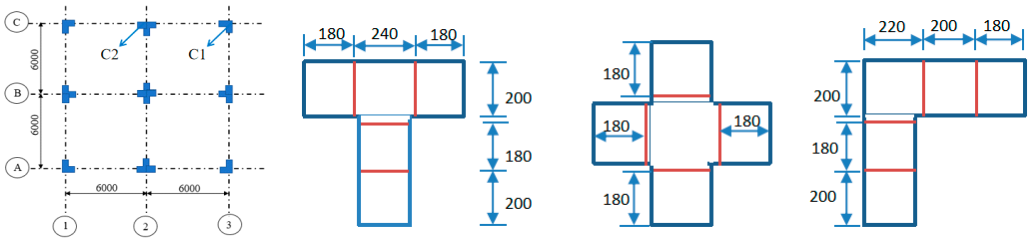

Figure 3. Frame layout and sections.

Table 3. Component information.

Component Type	Section Size	Concrete	Steel Strength Grade and Others
Main beam	$b_c \times h_c$ = 200 mm × 600 mm	C40	Reinforcement ratio 2%
T-shaped side pillar L-shaped corner post Cross-shaped newel	$h \times b \times t_s$ = 600 mm × 200 mm × 8 mm $h \times b \times t_s$ = 600 mm × 200 mm × 8 mm $h \times b \times t_s$ = 600 mm × 600 mm × 8 mm		Steel pipeQ345 Stiffening steel barsHPB300 Diameter 6 mm Longitudinal spacing 100 mm
Foundation	2 m × 2 m × 1 m (Buried deep 1 m)		Reinforcement ratio 2%

* h is the height of the column limb; b is the thickness of the column limb; t_s is the thickness of the steel pipe; b_c is the width of the concrete beam; h_c is the width of the concrete beam.

3.1. Temperature Field Model

The thermal parameters of the material, the heat conduction mode, the contact thermal resistance between the concrete and steel pipe in the concrete-filled steel tube columns, and the unit types of the steel pipe, concrete, and steel bars in the concrete-filled steel tube columns were consistent with the temperature field finite element model in Section 2.2, and the structural grid is 30 mm. The temperature was raised at the bottom of the structure, the adiabatic boundary conditions were set above the second floor, and the heating time was set to 30 min and 60 min, respectively. The temperature field calculation cloud diagram of the structure is shown in Figure 4.

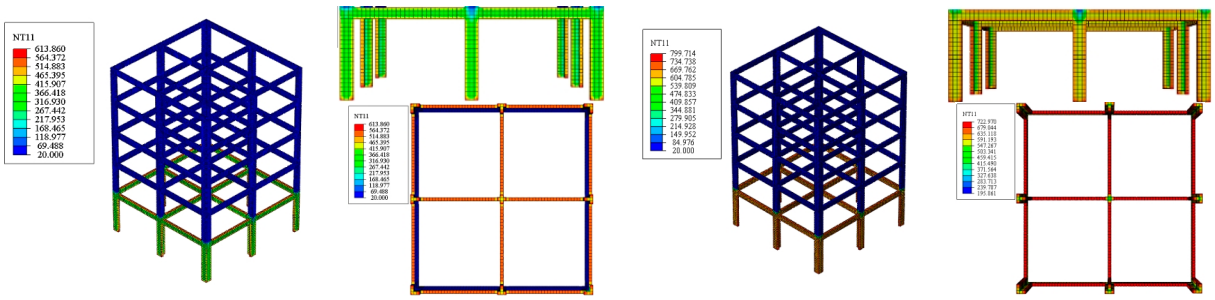

Figure 4. Cloud diagram of temperature field calculation: (**a**) Bottom heats up 30 min; (**b**) Bottom heats up 60 min.

3.2. Mechanical Field Model

3.2.1. Steel Pipe, Steel Bar, Concrete Constitutive

(1) Steel pipe

The elastic modulus of the steel pipe at normal temperature was taken as 2×10^5 MPa. After high temperature, the elastic modulus of the steel pipe was adopted from the literature [35].

$$E_s(T_{max}) = \begin{cases} E_s & T_{max} \le 500\ ^\circ\mathrm{C} \\ \left[1 - 1.30 \times 10^{-4} \times (T_{max} - 500)\right] \times E_s & T_{max} > 500\ ^\circ\mathrm{C} \end{cases} \quad (1)$$

where $E_s(T_{max})$ is elastic modulus of steel after high temperature; T_{max} is the highest temperature of the steel tube in the process of rising and cooling.

The stress–strain relationship of the steel pipe adopted the secondary plastic flow model:

$$\sigma_s = \begin{cases} E_s\varepsilon_s & \varepsilon_s \le \varepsilon_e \\ -A\varepsilon_s^2 + B\varepsilon_s + C & \varepsilon_e < \varepsilon_s \le \varepsilon_{e1} \\ f_y & \varepsilon_{e1} < \varepsilon_s \le \varepsilon_{e2} \\ f_y[1 + 0.6(\varepsilon_s - \varepsilon_{e2})/(\varepsilon_{s3} - \varepsilon_{e2})] & \varepsilon_{e2} < \varepsilon_s \le \varepsilon_{e3} \\ 1.6f_y & \varepsilon_s > \varepsilon_{e3} \end{cases} \quad (2)$$

where $\varepsilon_e = 0.8f_y/E_s$; $\varepsilon_{e1} = 1.5\varepsilon_e$; $\varepsilon_{e2} = 10\varepsilon_{e1}$; $\varepsilon_{e3} = 100\varepsilon_{e1}$; $A = 0.2f_y/(\varepsilon_{e1} - \varepsilon_e)^2$; $B = 2A\varepsilon_{e1}$; $C = 0.8f_y + A\varepsilon_{e2} - B\varepsilon_e$.

The yield strength of steel pipe after high temperature was adopted from the literature [35]:

$$f_y(T_{max}) = \begin{cases} f_y & T_{max} \le 500\ ^\circ\mathrm{C} \\ \left[1 - 2.33 \times 10^{-4} \times (T_{max} - 500) - 3.88 \times 10^{-7} \times (T_{max} - 500)^2\right] \times f_y & T_{max} > 500\ ^\circ\mathrm{C} \end{cases} \quad (3)$$

(2) Steel bar

The elastic modulus of steel bars at room temperature and high temperature was consistent with that of steel pipe. The stress–strain of the steel bars adopted the ideal

elastic-plastic model, and the yield strength of the steel bars after high temperature was adopted from [35]:

$$f_b(T_{max}) = \begin{cases} f_b & T_{max} \le 500\ ^\circ C \\ \left[1 - 5.82 \times 10^{-4} \times (T_{max} - 500)\right] \times f_b & T_{max} > 500\ ^\circ C \end{cases} \quad (4)$$

where f_b is the yield strength of steel bars.

(3) Concrete

The elastic modulus of concrete at normal temperature was determined by the recommended formula of ACI 318 (2011) [36]:

$$E_c = 4700\sqrt{f_c'} \quad (5)$$

where f_c' is the compressive strength of concrete cylinder.

The elastic modulus of concrete after high temperature adopted the formula suggested by [37]:

$$E_c(T_{max}) = \begin{cases} (100 - 0.0744T_{max}) \times 10^{-2} E_c & 0\ ^\circ C < T_{max} \le 300\ ^\circ C \\ (127.54 - 0.1662T_{max}) \times 10^{-2} E_c & 300\ ^\circ C < T_{max} \le 700\ ^\circ C \\ 0.11E_c & 700\ ^\circ C < T_{max} \le 900\ ^\circ C \end{cases} \quad (6)$$

Ref. [38] recommends the selection of the compressive stress–strain relationship of concrete after high temperature:

$$\sigma_c = \begin{cases} \sigma_{co}\left[A(\varepsilon_c/\varepsilon_{co}) - B(\varepsilon_c/\varepsilon_{co})^2\right] & \varepsilon_c \le \varepsilon_{co} \\ \sigma_{co}(\varepsilon_c/\varepsilon_{co}) / \left[\beta(\varepsilon_c/\varepsilon_{co} - 1)^{\eta} + \varepsilon_c/\varepsilon_{co}\right] & \varepsilon_c > \varepsilon_{co} \end{cases} \quad (7)$$

$$\sigma_{co} = f_{ck}\left[1.194 + 0.25(13/f_{ck})^{0.45}\left(-0.07845\xi^2 + 0.5789\xi\right)\right] \quad (8)$$

$$\varepsilon_{co} = 1300 + 14.93f_{ck} + 0.95\left[1400 + 800\left(\frac{f_{ck} - 20}{20}\right)\right]\xi^{0.2} \quad (9)$$

$$\eta = 1.60 + 1.5(\varepsilon_\infty/\varepsilon_c) \quad (10)$$

$$A = 2.0 - k \quad (11)$$

$$B = 1.0 - k \quad (12)$$

$$k = 0.1\xi^{0.745} \quad (13)$$

$$\xi = \frac{A_s f_y}{A_c f_{ck}} \quad (14)$$

$$\beta = \begin{cases} \frac{0.75 f_{ck}^{0.1}}{\sqrt{1+\xi}} & \xi \le 3.0 \\ \frac{0.75 f_{ck}^{0.1}}{\sqrt{1+\xi}(\xi-2)^2} & \xi > 3.0 \end{cases} \quad (15)$$

where σ_{co} is peak stress of the concrete at normal temperature, unit is MPa; ε_{co} is the peak strain of the concrete at normal temperature, unit is MPa; f_{ck} is the axial compressive strength of the concrete cube, unit is MPa; f_y is the yield strength of the steel, in MPa; ξ is the restraint effect coefficient of the steel pipe on the concrete; A_S and A_C are the areas of the steel tube and the core concrete, respectively. ξ is the constraint effect coefficient of the steel tube on the concrete.

The peak stress and peak strain of the concrete after high temperature was adopted from the formula recommended by [38]:

$$\sigma_{co}(T_{max}) = \frac{\sigma_{co}}{1 + 2.4(T_{max} - 20)^6 \times 10^{-17}} \quad (16)$$

$$\varepsilon_{co}(T_{max}) = \left[1 + \left(1500T_{max} + 5T_{max}^2\right) \times 10^{-16}\right]\varepsilon_{co} \quad (17)$$

where $\sigma_{co}(T_{max})$ is the peak stress of the concrete after high temperature, unit is MPa; $\varepsilon_{co}(T_{max})$ is the peak strain of the concrete after high temperature, unit is MPa.

The tensile stress–strain relationship of the concrete after high temperature adopted the recommendation of [39]. Assume that the initial elastic modulus of concrete under tension is the same as that under compression, and $f_t = 0.09f_c'$. At this time, the reduction formula of compressive strength $f_{c'}$ after high temperature is:

$$f_c'(T_{max}) = \frac{f_c'}{1 + 2.4(T_{max} - 20)^6 \times 10^{-17}} \quad (18)$$

3.2.2. Soil Constitutive and Parameters

The soil adopts the M-C model, and the parameters are shown in Table 4. Medium-hard, medium-soft and soft soils correspond to category II, III and IV sites, respectively.

Table 4. Soil parameters.

Venue Type	Density kg/m^3	Initial Shear Modulus 10^4 kPa	Effective Shear Modulus 10^4 kPa	Poisson Ratio	Shear Wave Speed m/s	Internal Friction Angle °	Cohesion kPa
Medium hard soil	1800	28.8	12.096	0.30	400	30	60
Medium soft soil	1700	6.8	2.856	0.35	200	12	25
Weak soil	1600	3.6	1.512	0.40	150	5	20

3.2.3. Element Types, Meshing, Computational Domains and Boundaries

The steel pipe, concrete, reinforcing steel bars, foundations, soil, and boundaries adopt S4R, C3D8R, T3D2, C3D8R, and C3D8R unit types, respectively. The meshing of the mechanical field and the temperature field should be consistent to ensure one-to-one correspondence between the nodes of the mechanical field and temperature field units. The meshing of the superstructure should be 30 mm. The calculation domain is 95 m × 95 m × 20 m, and the soil grid is divided into 3 m, as shown in Figure 5.

3.2.4. Contact Settings between Steel Pipe and Concrete, Foundations and Foundations, Steel Bars and Steel Pipe, Steel Bars and Concrete

The contact between the steel pipe and concrete and the contact between the foundation and foundation adopt the surface-to-surface contact pairs. The normal direction is hard contact and the tangential direction is Coulomb friction. The friction coefficient between the steel pipe and concrete is 0.6 at normal temperature and 0.25 post fire. The friction coefficient between the foundation and foundation is 0.3 [39]. The interaction between the steel bars and steel pipe is bounded by binding constraints, and the interaction between the steel bars and concrete is embedded by constraints.

3.2.5. Seismic Waves, Viscoelastic Boundaries and Damping

The El-Centro was selected as the input seismic wave, with a duration of 15 s and a frequency band concentrated at 0.3–20 Hz (low-pass filtering). The acceleration time history curve of the seismic wave was amplitude modulated to 0.70 m/s^2 and 2.0 m/s^2, corresponding to a = 0.07 g, respectively, and a = 0.20 g. The viscoelastic boundary thickness is 5 m, see Figure 5. Boundary parameters $\alpha_T = 0.667$, $\alpha_N = 1.333$. The soil damping ratio is 0.02, and the structural damping ratio is 0.05.

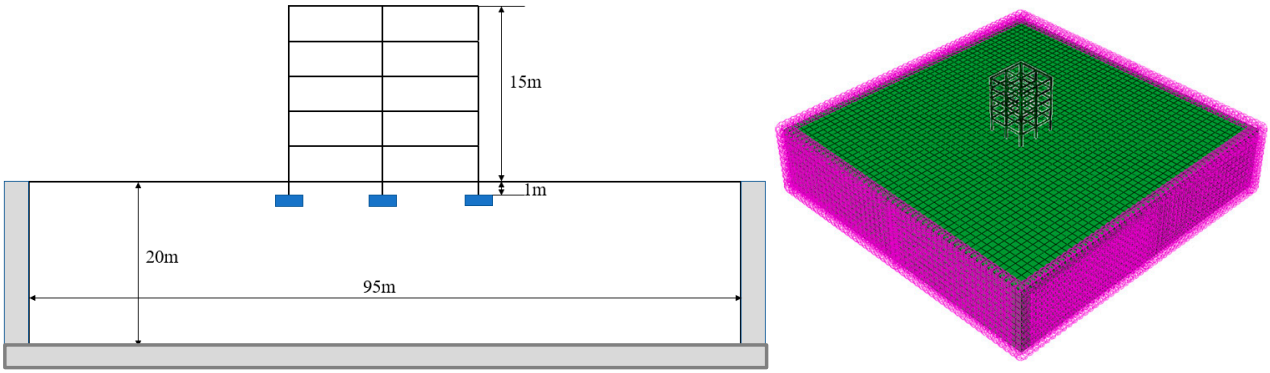

Figure 5. Compute Fields and boundaries.

4. Analysis on Seismic Performance of Stiffened Thin-Walled Special-Shaped Steel Tube Concrete Frame Structure Post Fire Considering the SSI

4.1. Natural Periods of Vibration

Figure 6 shows the calculation results of the basic natural vibration period of the structure under different site conditions and after being exposed to fire.

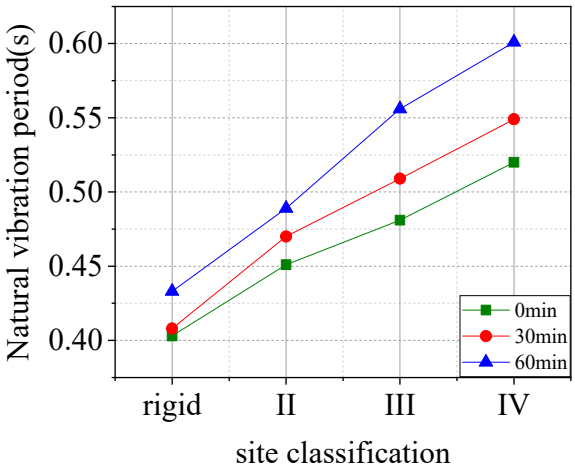

Figure 6. Natural vibration period of the structure before and post fire.

It can be seen that since the high-temperature damage of the material after the fire reduces the structural stiffness, the natural vibration period after the fire will increase; the research results show that the axial compression stiffness of the concrete-filled steel tube column after the fire decreases by 5% with the fire time (30–180 min)~40%, so when the local fire time is short, the stiffness of the structure decreases to a small extent, so the natural vibration period of the structure increases slightly, around 2–10%.

4.2. Maximum Acceleration

Under different foundation conditions, the acceleration time history curves (Figure 3) of the top corner column C1 and center column C2 are shown in Figures 7–10. The maximum acceleration and occurrence time of the vertices of pillars 1 and 2 on the top floor are shown in Table 5.

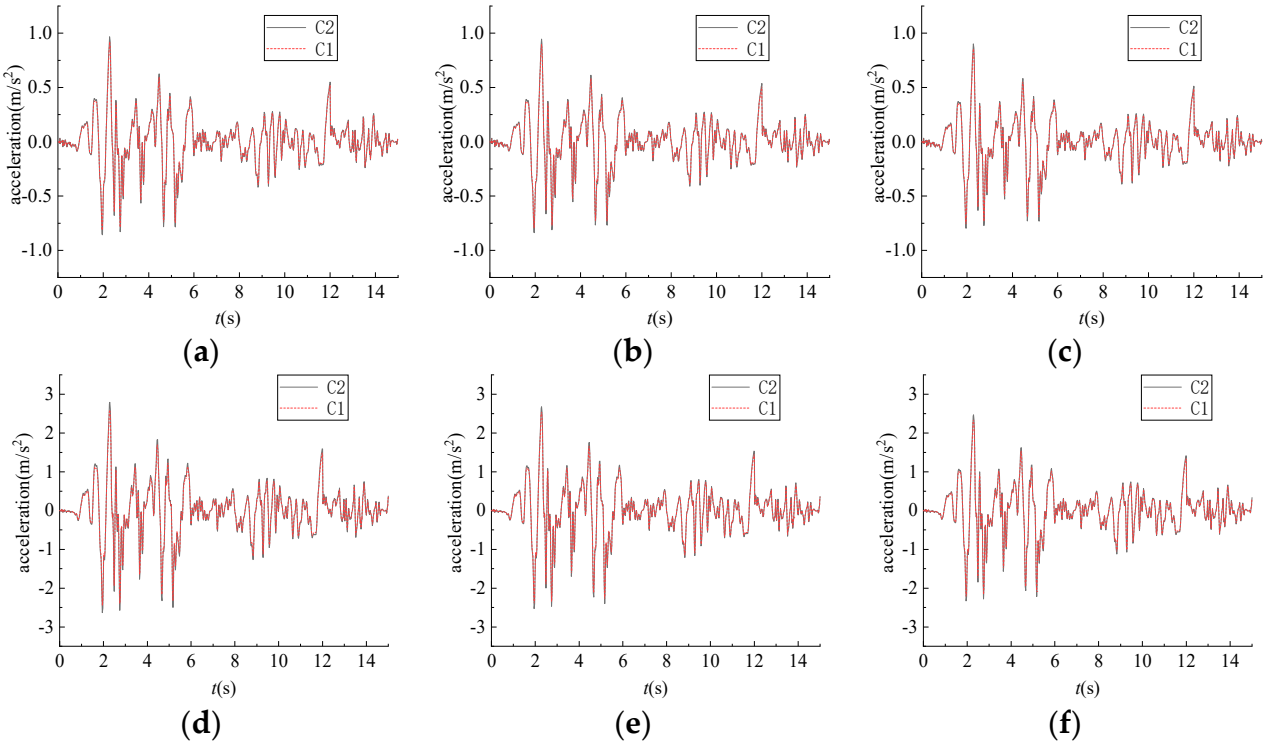

Figure 7. Acceleration time on top of columns 1 and 2 under the condition of rigid foundation: (**a**) Without fire, a = 0.07 g; (**b**) With fire 30 min, a = 0.07 g; (**c**) With fire 60 min, a = 0.07 g; (**d**) Without fire, a = 0.20 g; (**e**) With fire 30 min, a = 0.20 g; (**f**) With fire 60 min, a = 0.20 g.

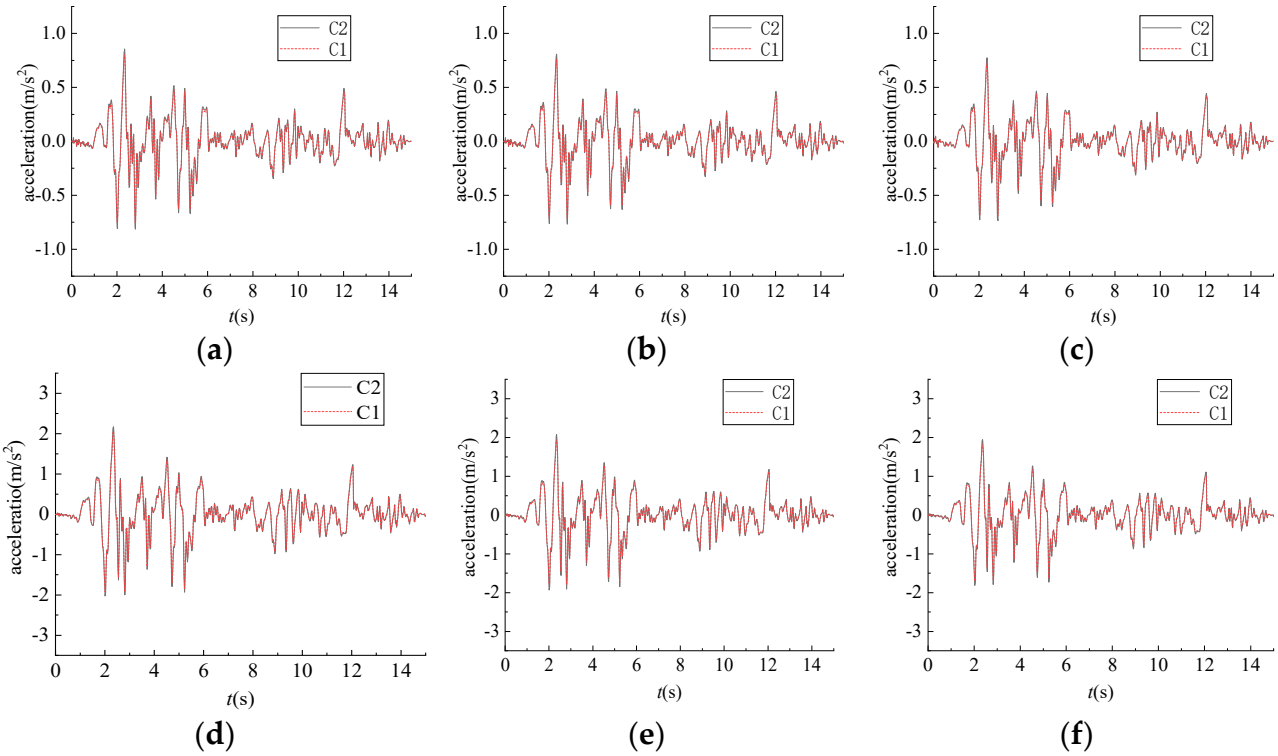

Figure 8. Acceleration time on top of columns 1 and 2 under class II foundation conditions: (**a**) Without fire, a = 0.07 g; (**b**) With fire 30 min, a = 0.07 g; (**c**) With fire 60 min, a = 0.07 g; (**d**) Without fire, a = 0.20 g; (**e**) With fire 30 min, a = 0.20 g; (**f**) With fire 60 min, a = 0.20 g.

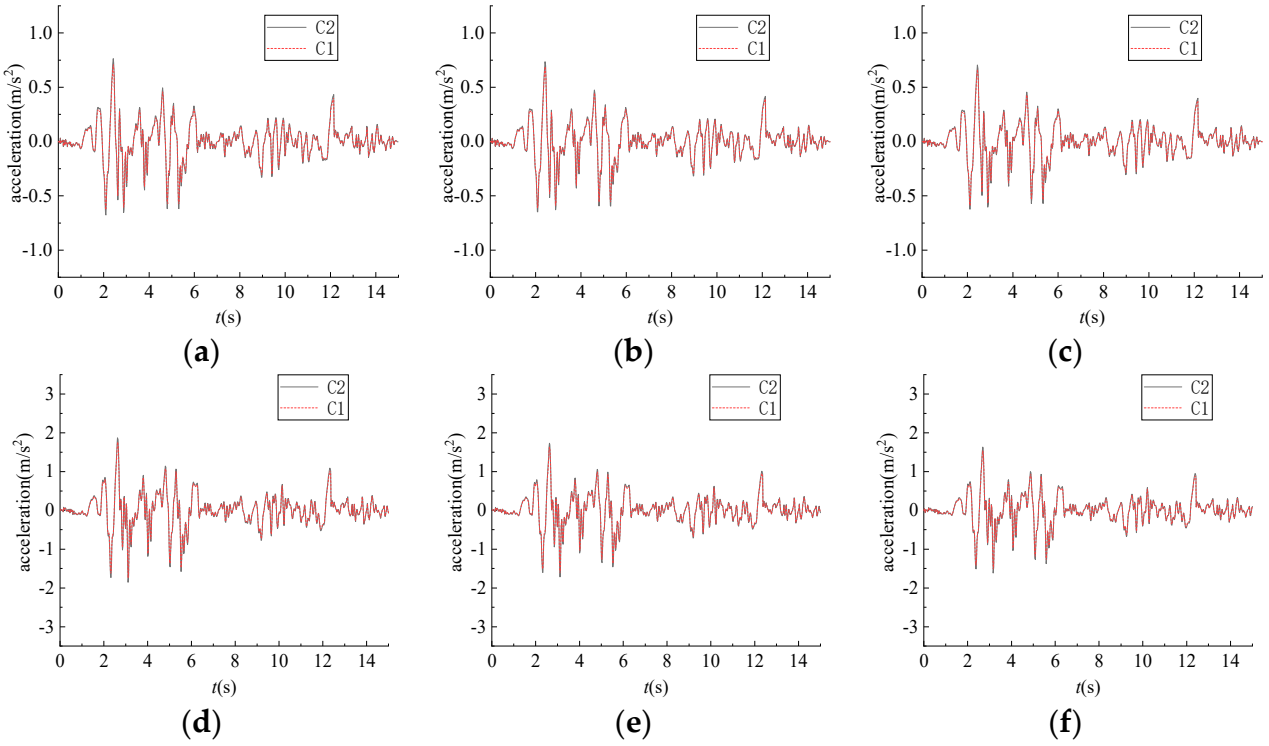

Figure 9. Acceleration time on top of columns 1 and 2 under class III foundation conditions: (**a**) Without fire, a = 0.07 g; (**b**) With fire 30 min, a = 0.07 g; (**c**) With fire 60 min, a = 0.07 g; (**d**) Without fire, a = 0.20 g; (**e**) With fire 30 min, a = 0.20 g; (**f**) With fire 60 min, a = 0.20 g.

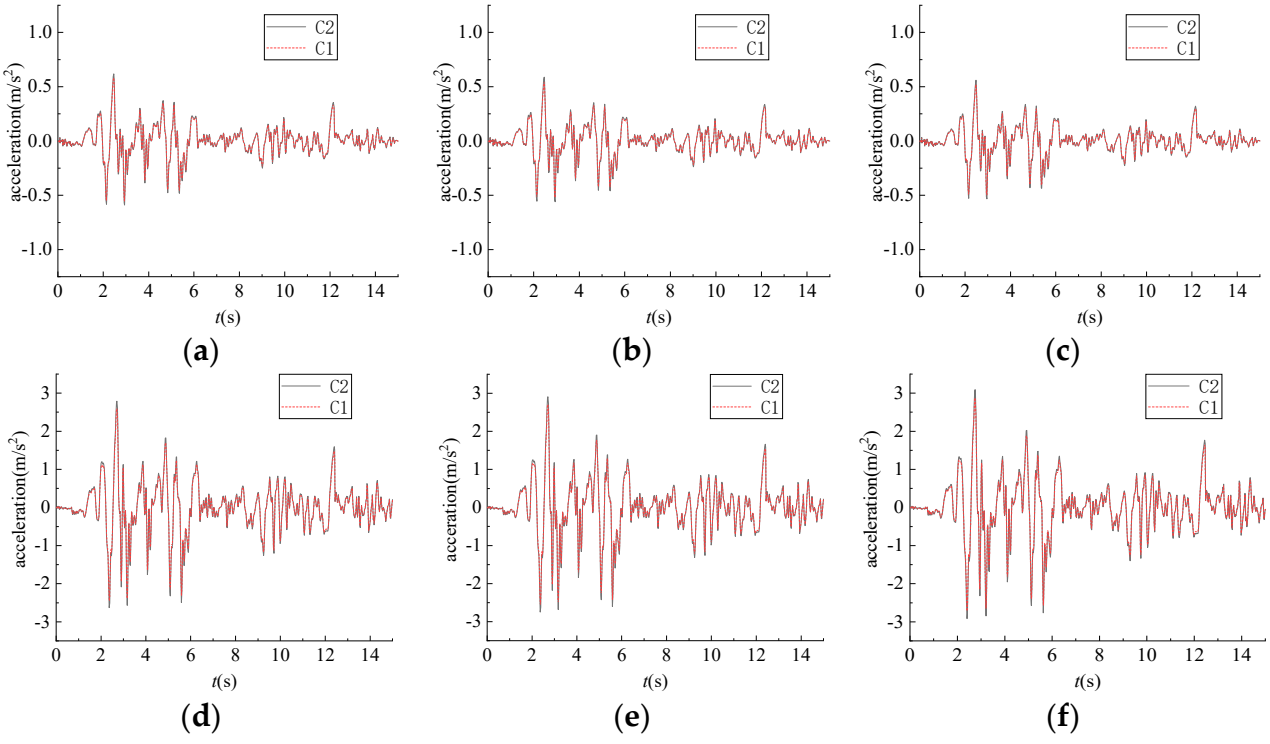

Figure 10. Acceleration time on top of columns 1 and 2 under class IV foundation conditions: (**a**) Without fire, a = 0.07 g; (**b**) With fire 30 min, a = 0.07 g; (**c**) With fire 60 min, a = 0.07 g; (**d**) Without fire, a = 0.20 g; (**e**) With fire 30 min, a = 0.20 g; (**f**) With fire 60 min, a = 0.20 g.

Table 5. Maximum acceleration and occurrence time of top column 1 and column 2.

Acceleration Amplitude	Bar Position	Fire Conditions	Rigid Foundation		Category II Venue		Category III Venue		Category IV Venue	
			Acceleration	Time	Acceleration	Time	Acceleration	Time	Acceleration	Time
0.07 g	1	Without fire	0.967	2.342	0.857	2.365	0.764	2.381	0.619	2.400
		With fire 30 min	0.946	2.350	0.808	2.375	0.734	2.395	0.588	2.415
		With fire 60 min	0.901	2.356	0.774	2.385	0.705	2.418	0.560	2.440
	2	Without fire	0.953	2.339	0.845	2.396	0.762	2.416	0.618	2.436
		With fire 30 min	0.921	2.371	0.787	2.363	0.716	2.378	0.567	2.398
		With fire 60 min	0.871	2.363	0.748	2.392	0.702	2.425	0.545	2.448
0.20 g	1	Without fire	2.789	2.352	2.171	2.388	1.871	2.429	2.788	2.491
		With fire 30 min	2.676	2.360	2.076	2.398	1.733	2.446	2.910	2.511
		With fire 60 min	2.470	2.367	1.954	2.409	1.632	2.484	3.091	2.545
	2	Without fire	2.750	2.349	2.141	2.420	1.867	2.432	2.782	2.495
		With fire 30 min	2.606	2.382	2.022	2.386	1.691	2.451	2.806	2.526
		With fire 60 min	2.388	2.374	1.890	2.416	1.625	2.493	3.008	2.559

It can be seen that (1) The acceleration time history curves of the top corner column 1 and the center column 2 are nearly coincident, which indicates that the structure is dominated by translational motion. Since the structure itself is a symmetrical regular structure, the temperature field is symmetrical only when the ground floor is exposed to fire, so the acceleration time histories of the corner columns and side columns nearly overlap; (2) Compared with the center column 2, the stress on the corner column 1 is more complex. Therefore, the maximum acceleration is slightly higher; (3) The peak acceleration peak moments of corner column 1 and top column 2 are basically the same, which is consistent with the vibration characteristics of regular structures; (4) Under different site conditions, consider that the maximum acceleration peak moment of the SSI has a hysteresis, and as the amplitude of ground motion increases, the degree of nonlinear development of soil increases. The longer the fire exposure time, the more obvious the hysteresis; taking a Category III site as an example, when the seismic acceleration amplitude is 0.2 g, compared with not being exposed to fire, corner column 1 lags behind by 0.07 s and 0.055 s, respectively, after being exposed to fire for 30 min and 60 min. This is because the high temperature causes irreversible damage to the structure. Damage results in a reduction in structural stiffness and a reduction in the natural vibration period of the structure; since the fire time in this article is not long and the fire is local, the impact of fire conditions on the acceleration peak hysteresis is not obvious. Under unfired conditions, when the seismic acceleration amplitude is 0.2 g, under Category II, III, and IV site conditions, the peak acceleration moment of corner column 1 is 0.036 s, 0.077 s, and 0.139 s later than that under rigid foundation conditions, respectively. This is because the softer the soil, the greater the seismic acceleration amplitude, while the higher the degree of nonlinearity of the soil corresponds to the reduction in the natural vibration period of the structure and the more obvious the hysteresis of the acceleration peak.

Take the maximum acceleration of corner column 1 and its corresponding foundation bottom surface, see Figure 11. It can be seen that (1) Under the condition of rigid foundation, since the acceleration acts directly on the foundation, the foundation acceleration amplitude is close to the seismic wave acceleration amplitude. (2) As an example, the maximum acceleration of the structure and foundation considering the SSI in Category II and III sites is less than the calculation result of rigid foundation, indicating that the internal force of the structure calculated based on the assumption of rigid foundation is biased toward safety at this time. In Category IV sites, when a = 0.20 g, the maximum acceleration of the structure and foundation after considering the SSI is greater than the calculation result of rigid foundation, indicating that the SSI should be considered in the structural design at this time. That is, under different site conditions, the acceleration response of the structure and foundation is uncertain. The reason for this uncertainty is that the effect size of soil–structure interaction is not only related to seismic waves and site soil, but also

to the structure itself. When the bedrock seismic source is transmitted to the structure through the filtering and amplification effect of the site soil, when its spectrum is close to the spectrum of the structure, the acceleration response of the structure and foundation will be intensified; conversely, the acceleration response of the structure and foundation will be reduced. Since the EL-Centro seismic wave itself has a high low-frequency content, the low-frequency content is relatively rich when the site soil is IV, and the basic period of the structure is small (the frequency is between 2.0–2.5 HZ under different site conditions). Accordingly, the IV site soil not only increases the frequency of seismic waves but also amplifies most of the low-frequency components to a greater extent, which in turn leads to an increase in the acceleration response of foundations and structures. (3) Since the gravity load value of each floor is close, the maximum acceleration of each floor increases with the increase in floor height, and the maximum acceleration response of the structure appears on the top floor. (4) Material deterioration post fire causes structural stiffness degradation, so the maximum acceleration of the structure post fire is smaller than that of the unfired structure.

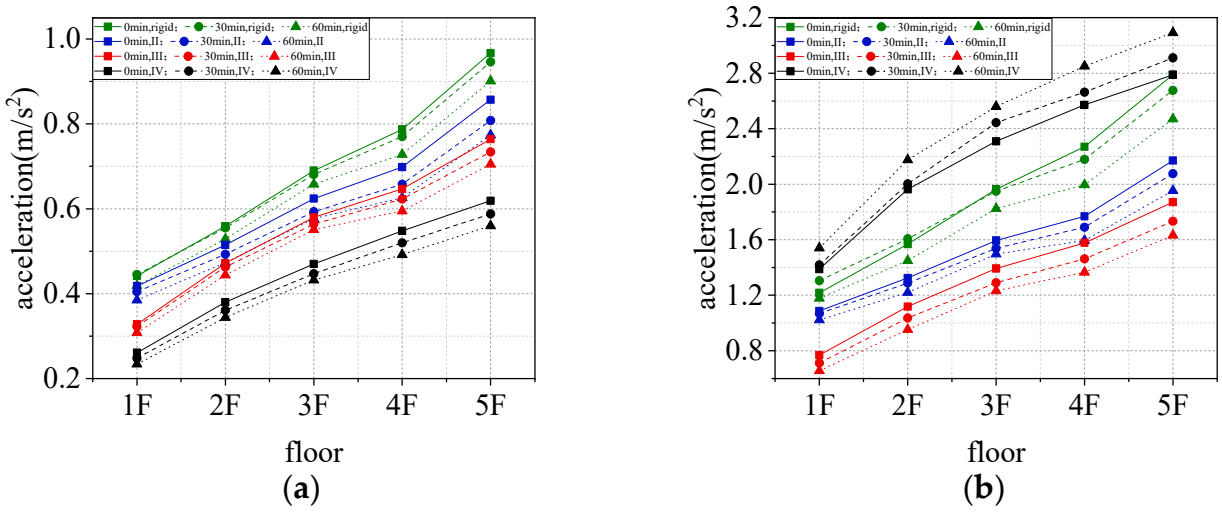

Figure 11. The maximum accelerations of structure: (**a**) a = 0.07 g; (**b**) a = 0.20 g.

4.3. Interlaminar Shear

Figure 12 shows the variation trend of the maximum inter-story shear force of each layer under different site conditions. The maximum inter-story shear force depends on the maximum acceleration response and mass. Since the mass of each floor of the model is basically the same, the changing trend of the shear force is consistent with the maximum acceleration.

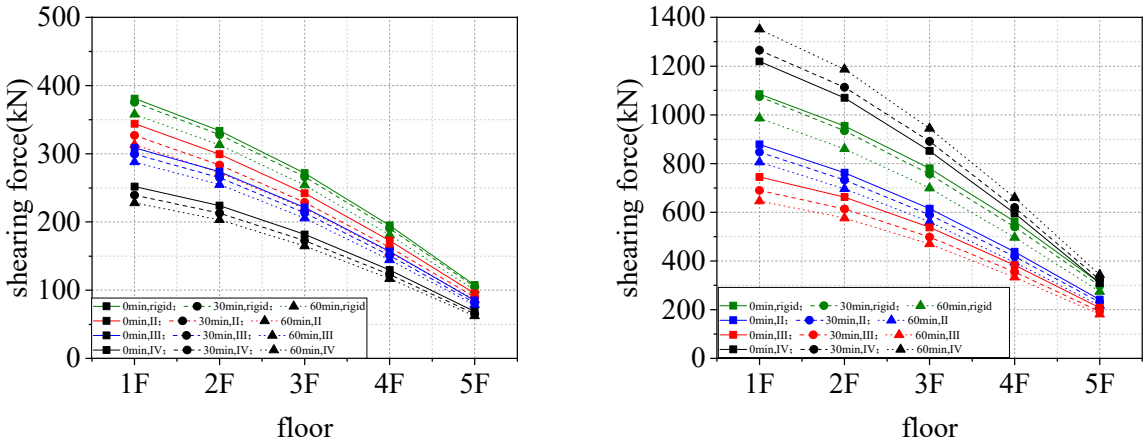

Figure 12. Shearing force of floor.

4.4. Maximum Inter-Story Displacement Angle

Table 6 shows the maximum inter-story displacement angle of the structure. It can be seen that (1) Compared with the rigid foundation, the inter-story displacement angle will increase after considering the SSI. This is because the inter-story displacement angle composition of the two is different. For regular structures, after considering the SSI, the inter-story displacement angle caused by the deformation of the structure itself is excluded. In addition to the rotation angle, there are also rotation angles caused by foundation rotation, so the inter-story displacement angle considering soil–structure interaction will increase. In addition, the softer the soil and the greater the earthquake magnitude, the higher the proportion of the inter-story displacement angle caused by foundation rotation in the total deformation. (2) Under the same site conditions, when not exposed to fire, the maximum inter-story shear force gradually accumulates from top to bottom, causing the maximum inter-story shear force to appear on the bottom layer, and the lateral movement stiffness of the bottom layer frame in this example is smaller than that of other layers. Accordingly, the maximum inter-story displacement angle occurs at the bottom of the structure; when the bottom layer is exposed to fire for 30 min, the stiffness of the bottom layer of the structure is reduced due to the high temperature, so the inter-story displacement angle of the bottom layer is significantly increased compared to the case where it is not exposed to fire; when a = 0.07 g, it increases about 10%; when a = 0.20 g, it increases by about 20%. When the bottom layer is exposed to fire for 60 min, the stiffness of the bottom layer of the structure decreases and intensifies, so the inter-story displacement angle of the bottom layer increases more significantly; when a = 0.07 g, it increases by about 20%; when a = 0.20 g, it increases by about 35%. (3) When a = 0.07 g, the inter-story displacement angle is <1/250, and the structure is basically intact or slightly damaged; when a = 0.20 g, most of the inter-story displacement angles meet <1/100, and the structure is moderately damaged. The scope of the calculation example shows that the structure has the value of repairing after the fire when the fire area is not large, the time is not long, and the earthquake is less than moderate.

Table 6. Maximum inter-story displacement Angle of each story of the structure.

Fire Exposure Time	Location	Seismic Wave Amplitude a = 0.07 g				Seismic Wave Amplitude a = 0.20 g			
		Rigid Foundation	Medium Hard Soil	Medium Soft Soil	Weak Soil	Rigid Foundation	Medium Hard Soil	Medium Soft Soil	Weak Soil
Without fire	5	0.039%	0.068%	0.098%	0.152%	0.134%	0.221%	0.464%	0.434%
	4	0.071%	0.097%	0.124%	0.177%	0.244%	0.319%	0.552%	0.558%
	3	0.100%	0.122%	0.148%	0.198%	0.338%	0.407%	0.629%	0.669%
	2	0.122%	0.143%	0.167%	0.215%	0.414%	0.481%	0.691%	0.764%
	1	0.140%	0.160%	0.180%	0.226%	0.470%	0.539%	0.732%	0.828%
With fire 30 min	5	0.039%	0.066%	0.097%	0.151%	0.139%	0.215%	0.456%	0.449%
	4	0.071%	0.093%	0.122%	0.174%	0.252%	0.309%	0.538%	0.586%
	3	0.098%	0.117%	0.145%	0.194%	0.353%	0.395%	0.609%	0.709%
	2	0.127%	0.143%	0.169%	0.215%	0.459%	0.486%	0.683%	0.841%
	1	0.147%	0.167%	0.189%	0.231%	0.496%	0.570%	0.743%	0.951%
With fire 60 min	5	0.045%	0.076%	0.115%	0.174%	0.155%	0.245%	0.531%	0.603%
	4	0.072%	0.105%	0.148%	0.205%	0.277%	0.356%	0.622%	0.782%
	3	0.105%	0.133%	0.179%	0.222%	0.374%	0.453%	0.711%	0.956%
	2	0.143%	0.162%	0.202%	0.255%	0.496%	0.551%	0.801%	1.137%
	1	0.174%	0.207%	0.230%	0.296%	0.633%	0.690%	0.921%	1.358%

5. Conclusions

On the basis of the finite element model of an irregular thin-walled steel tube concrete frame structure considering the SSI after a fire (with the bottom floor exposed to fire for 30 min and 60 min), this study conducted a dynamic response analysis. The main conclusions are as follows:

(1) After considering soil–structure interaction, the presence of the foundation increases the flexibility of the structure, leading to an increase in the natural periods of vibration. This effect is more pronounced when the soil is softer. Under the same site conditions, the elevated temperature reduces the structural stiffness, resulting in an increase by about 2–10% in the natural periods of vibration after fire. The longer the exposure

time to fire and the softer the soil, the more noticeable the increase in the natural periods of vibration for the structure.

(2) Compared to the results calculated under the assumption of a rigid foundation, the increase or decrease in the structural and foundation accelerations considering the soil-structure interaction introduces uncertainty. Generally, results based on the assumption of a rigid foundation tend to overestimate the values by about 0.5–13%. However, when the acceleration amplitude is 2.0 g and the fire time is 60 min, the acceleration amplitude of the top column 1 and column 2 increases by 9.49% on average, which indicates that the calculated structural dynamic response may be unsafe without consideration of the SSI. Therefore, it is recommended to consider the effect of SSI on the seismic performance of the structure when the fire time is more than 60 min in the soft soil site.

(3) The variation trend of inter-story shear force is primarily determined by the accelerations of the structure and foundation.

(4) The maximum inter-story displacement angle occurs at the bottom of the structure and is influenced by factors such as site conditions, seismic wave acceleration amplitudes, fire exposure conditions, and the maximum inter-story shear force in the structure. Softer soil, higher seismic wave acceleration amplitudes, and more pronounced fire effects lead to larger inter-story displacement angles, and the increase ranges from 10% to 35%, but all of them are no more than 1/100. In the case of small and moderate earthquakes, where the fire effect is relatively small, the structure is generally in the elastic or elastic-plastic stage, indicating potential for post-disaster recovery.

Currently, experimental research on seismic performance considering the SSI effects is primarily focused on concrete structures and steel frame structures. Further experimental studies on other structural systems and materials are needed. In addition, under the influence of rare seismic events, the goal of seismic design for structures is to prevent collapse. Due to the significantly increased probability of fire occurrence during rare seismic events, it is necessary to further investigate the post-fire structural collapse performance considering the SSI effects under such rare seismic events.

Author Contributions: W.W.: conceptualization, methodology, writing—original draft; X.L.: resources, writing—review and editing, Supervision; J.Z.: validation, writing—review and editing, funding acquisition; S.Y.: software, data curation, writing—review and editing; J.L.: formal analysis, investigation, writing—review and editing; Y.Y.: conceptualization, writing—review and editing, project administration. All authors have read and agreed to the published version of the manuscript.

Funding: This research was funded by "Youth Program of National Natural Science Foundation of China, grant number 51208246" and "Guangdong Provincial Department of Education's Characteristic Innovation Project for Colleges and Universities, grant number 2023KTSCX218".

Data Availability Statement: Dataset available on request from the corresponding author.

Conflicts of Interest: The authors declare no conflicts of interest.

References

1. Tao, Z.; Han, L.-H.; Wang, D.-Y. Experimental behaviour of concrete-filled stiffened thin-walled steel tubular columns. *Thin-Walled Struct.* **2007**, *45*, 517–527. [CrossRef]
2. Li, M.; Zong, Z.; Hao, H.; Zhang, X.; Lin, J.; Xie, G. Experimental and numerical study on the behaviour of cfdst columns subjected to close-in blast loading. *Eng. Struct.* **2019**, *185*, 203–220. [CrossRef]
3. Wang, X.-T.; Xie, C.-D.; Lin, L.-H.; Li, J. Seismic behavior of self-centering concrete-filled square steel tubular (cfst) column base. *J. Constr. Steel Res.* **2019**, *156*, 75–85. [CrossRef]
4. Lyu, X.; Xu, Y.; Xu, Q.; Yu, Y. Axial compression performance of square thin walled concrete-Filled steel tube stub columns with reinforcement stiffener under constant high-Temperature. *Materials* **2019**, *12*, 1098. [CrossRef] [PubMed]
5. Li, R.; Yu, Y.; Samali, B.; Li, C. Parametric analysis on the circular CFST column and RBS steel beam joints. *Materials* **2019**, *12*, 1513. [CrossRef] [PubMed]
6. Liu, X.; Xu, C.; Liu, J.; Yang, Y. Research on special-shaped concrete-filled steel tubular columns under axial compression. *J. Constr. Steel Res.* **2018**, *147*, 203–223. [CrossRef]

7. Zhang, J.; Li, Y.; Zheng, Y.; Wang, Z. Seismic damage investigation of spatial frames with steel beams connected to l-shaped concrete-filled steel tubular (cfst) columns. *Appl. Sci.* **2018**, *8*, 1713. [CrossRef]
8. Zhou, X. Analysis of Seismic Performance of Concrete-Filled Steel Tube Special-Shaped Column Frame Structure System. Master's Thesis, Chongqing University, Chongqing, China, 2020.
9. Jiang, H. Research on the Seismic Performance of Prefabricated Concrete-Filled Steel Tube Special-Shaped Column Frame Structure. Master's Thesis, North China University of Science and Technology, Tangshan, China, 2021.
10. Li, X.; Xu, Z.; Bao, Y.; Cong, Z. Post-fire seismic behavior of two-bay two-story frames with high-performance fiber-reinforced cementitious composite joints. *Eng. Struct.* **2019**, *183*, 150–159. [CrossRef]
11. Xiong, Y.; Chen, A.; Wu, D.; Zhao, G. Seismic performance of composite shear walls filled with demolished concrete lumps and self-compacting concrete after fire. *Buildings* **2022**, *12*, 1308. [CrossRef]
12. Ni, S.; Birely, A.C. Simulation procedure for the post-fire seismic analysis of reinforced concrete structural walls. *Fire Saf. J.* **2018**, *95*, 101–112. [CrossRef]
13. Demir, U.; Goksu, C.; Binbir, E.; Ilki, A. Impact of time after fire on post-fire seismic behavior of rc columns. *Structures* **2020**, *26*, 537–548. [CrossRef]
14. Qian, S.; Qian, X.; Sun, Y.; Mao, X.; Liu, T.; Huan, Y. Analysis of post-fire seismic performance of multi-story RC frames under near-fault earthquakes. *Earthq. Eng. Eng. Dyn.* **2021**, *41*, 219–227.
15. Pan, Y. Study on Seismic Performance of Concrete Frames after Local Fire. Master's Thesis, Shenyang Jianzhu University, Shenyang, China, 2022.
16. Yu, Y.; Zhang, C.; Xie, X.; Yousefi, A.M.; Zhang, G.; Li, J.; Samali, B. Compressive strength evaluation of cement-based mate-rials in sulphate environment using optimized deep learning technology. *Dev. Built Environ.* **2023**, *16*, 100298. [CrossRef]
17. Yu, Y.; Hoshyar, A.N.; Samali, B.; Zhang, G.; Rashidi, M.; Mohammadi, M. Corrosion and coating defect assessment of coal handling and preparation plants (CHPP) using an ensemble of deep convolutional neural networks and decision-level data fusion. *Neural Comput. Appl.* **2023**, *35*, 18697–18718. [CrossRef]
18. Rabi, M.; Cashell, K.A.; Shamass, R. Ultimate behaviour and serviceability analysis of stainless steel reinforced concrete beams. *Eng. Struct.* **2021**, *248*, 113259. [CrossRef]
19. Rabi, M.; Cashell, K.A.; Shamass, R. Flexural analysis and design of stainless steel reinforced concrete beams. *Eng. Struct.* **2019**, *198*, 109432. [CrossRef]
20. Wang, J.H.; Kunnath, S.; He, J.; Xiao, Y. Post-earthquake fire resistance of circular concrete-filled steel tubular columns. *J. Struct. Eng.* **2020**, *146*, 04020105. [CrossRef]
21. Jiang, H.; Wang, X.; He, S. Numerical simulation of impact tests on reinforced concrete beams. *Mater. Des.* **2012**, *39*, 111–120. [CrossRef]
22. Yang, J.; Lu, Z.; Li, P. Large-scale shaking table test on tall buildings with viscous dampers considering pile-soil-structure interaction. *Eng. Struct.* **2020**, *220*, 110960. [CrossRef]
23. Liu, S.; Lu, Z.; Li, P.; Ding, S.; Wan, F. Shaking table test and numerical simulation of eddy-current tuned mass damper for structural seismic control considering soil-structure interaction. *Eng. Struct.* **2020**, *212*, 110531. [CrossRef]
24. Deb Roy, S.; Pandey, A.; Saha, R. Shake table study on seismic soil-pile foundation-structure interaction in soft clay. *Structures* **2021**, *29*, 1229–1241. [CrossRef]
25. Li, P.; Xiao, J.; Yang, J.; Ding, Y. Dynamic response analysis of frame structure system considering SSI effect. *J. South China Univ. Technol. Nat. Sci. Ed.* **2023**, *51*, 139–148.
26. Ding, Y.; Nie, M.; Xu, Y. Shaking table test study on wind power tower model structure considering soil-structure interaction. *J. Civ. Eng* 2024. [CrossRef]
27. Huang, Y.; Gu, M.; El Naggar, M.H. Effect of soil-structure interaction on wind-induced responses of supertall buildings with large pile groups. *Eng. Struct.* **2021**, *243*, 112557. [CrossRef]
28. Sadek, M.; Hussein, M.; Hage Chehade, F.; Arab, A. Influence of soil–structure interaction on the fundamental frequency of shear wall structures. *Arab. J. Geosci.* **2020**, *13*, 877. [CrossRef]
29. Hamidia, M.; Shokrollahi, N.; Nasrolahi, M. Soil-structure interaction effects on the seismic collapse capacity of steel moment-resisting frame buildings. *Structures* **2021**, *32*, 1331–1345. [CrossRef]
30. Zhao, J.; Song, L.; Zhou, Z. Analysis of main and aftershock vulnerability of nuclear power plant SSC coupling system model considering SSI effect. *Nucl. Power Eng.* **2023**, *44*, 85–94.
31. He, J. Research on Seismic Response and Vibration Reduction of Space Structures Considering Soil-Structure Interaction. Master's Thesis, Tianjin University, Tianjin, China, 2017.
32. Liu, J.; Du, Y.; Yan, Q. Implementation of viscoelastic artificial boundary and ground motion input in general finite element software. *J. Disaster Prev. Mitig. Eng.* **2007**, *27*, 43–48.
33. Wang, W. Study on Post-Fire Seismic Performance of Special-Shaped Concrete-Filled Steel Tube Frame Structures Considering SSI Effect. Ph.D. Thesis, Liaoning Technical University, Fuxin, China, 2021.
34. *ENV 1994-1-2:2004*; Eurocode 4, 2004. Design of Composite Steel and Concrete Structures, Part 1: General Rules-Structural Fire Design. European Committee for Standardization: Brussels, Belgium, 2004.
35. Tao, Z.; Wang, X.-Q.; Uy, B. Stress-strain curves of structural and reinforcing steels after exposure to elevated temperatures. *J. Mater. Civ. Eng.* **2013**, *25*, 1306–1316. [CrossRef]

36. American Concrete Institute. *Building Code Requirements for Structural Concrete (ACI 318-11) and Commentary*; American Concrete Institute: Farmington Hills, MI, USA, 2011.
37. Xie, D.; Qian, Z. Experimental study on strength and deformation of concrete after exposure to high temperature (open flame). In Proceedings of the 5th National Structural Engineering Academic Conference, Haikou, China, 25–26 November 1996.
38. Han, L.-H.; Yang, Y.-F.; Yang, H.; Huo, J. Residual strength of concrete-filled rhs columns after exposure to the iso-834 standard fire. *Thin-Walled Struct.* **2002**, *40*, 991–1012. [CrossRef]
39. Hong, S.; Varma, A.H. Analytical modeling of the standard fire behavior of loaded cft columns. *J. Constr. Steel Res.* **2009**, *65*, 54–69. [CrossRef]